Finite Element Modeling of the Head Skeleton With a New Local Quantitative Assessment Approach

Barbara Autuori* , Karine Bruyère-Garnier, Fabrice Morestin, Michel Brunet, and Jean-Pierre Verriest

***Abstract*—The present study was undertaken to build a finite element model of the head skeleton and to perform a new assessment approach in order to validate it. The application fields for such an improved model are injury risk prediction as well as surgical planning. The geometrical reconstruction was performed using computed tomography scans and a total of 4680 shell elements were meshed on the median surface of the head skeleton with the particular characteristic of adapted mesh density and real element thickness. The assessment protocol of the finite element model was achieved using a quasi-static experimental compression test performed on the zygomatic bone area of a defleshed isolated head. Mechanical behavior of the finite element model was compared to the real one and the assessment approach was divided into two steps. First, the mechanical properties of the anatomical structure were identified using the simulation and then the simulated displacement field was compared to local displacement measurement performed during test using a digital correlation method. The assessment showed that the head skeleton model behaved qualitatively like the real structure. Quantitatively, the local relative error varied from 8% up to 70%.**

***Index Terms*—Biomechanics, compressive tests, finite element modeling, skull.**

I. Introduction

THE head skeleton is a complex structure whose specific architecture ensures the protection of cranial contents and sense organs. The principal causes of facial injuries are road accidents, falls, fight and sports activities [1]. Facial fractures observed in medical services concern mainly the nose, skull, mandible, zygomatic, and bones, and more rarely, orbits and maxilla [2]. In terms of threat to life [3], facial wounds are minor [4] whereas skull and brain injuries are severe and can be fatal to victims. This explains that skull fractures and brain injuries are commonly studied using experimentation or, more recently, by computational method whereas facial injuries are not.

Manuscript received August 12, 2004; revised September 25, 2005. This work was supported in part by the Medical Research Foundation. *Asterisk indicates corresponding author.*

*B. Autuori is with the Laboratory of Biomechanics and Human Modelling, INRETS of Bron, 25 Av. F. Mitterrand, case24, 69675 Bron Cedex, France (e-mail: barbara_autuori@yahoo.fr).

K. Bruyère-Garnier and J. P. Verriest are with the Laboratory of Biomechanics and Human Modelling, INRETS of Bron, 69675 Bron Cedex, France (e-mail: karine.bruyere@inrets.fr; jpv@inrets.fr).

F. Morestin and M. Brunet are with the Contact and Solid Mechanics Laboratory, INSA of Lyon, 69621 Villeurbanne Cedex, France (e-mail: Fabrice.Morestin@insa-lyon.fr; michel.brunet@insa-lyon.fr).

Digital Object Identifier 10.1109/TBME.2006.872812

Finite element modeling is a numerical method which allows for the reproduction of a particular loading on a structure, with varying parameters. Moreover, local mechanical parameters useful for phenomena characterization can be computed. For example, stress, as well as strain, is given by finite element models, whereas they can not easily be measured experimentally. The scope of applications for these finite element models of human body segments appears extremely wide; for the head they concern the following.

- Better understanding of injury mechanisms and pathological dysfunction.
- Injury risk prevention and protection, such as protection systems testing for road users (helmets), or fracture prevention of repaired bones.
- Surgical planning, such as in maxillofacial surgery cases which require force applications and bone displacements.

One may wonder if facial bone studies present much interest, considering the minor severity of facial injury when compared with brain injuries. Many arguments can be put forward to address this issue. First, in spite of their low life-threatening potential, facial fractures need several surgical acts to be repaired and they leave aesthetic as well as psychological sequels. Moreover, nowadays patients do not hesitate to resort to surgery in order to repair pathologic abnormalities or aesthetic traits, since aesthetic surgery has become common. Second, in view of injury prevention, finite element models of the head should have a realistic face, in order for brain injuries to be correctly predicted in the case of face impact. This is why facial bone modeling presents much relevance in various applications such as head injury prediction or surgical planning.

The facial bones have been experimentally studied by several authors, mainly in order to determine their tolerance to impact. For a particular bone tested, results found in these studies depend on experimental conditions. For drop tests on zygomatic bone, performed with plane contact surface, Nahum [5] found impact force tolerances equal to 890 N. When the head is isolated from the body and more rigidly fixed during impact, the force measured is slightly higher than the figures given above. Thus, force threshold for zygomatic bone found by Allsop [6] is 1737.5 N and Yoganandan *et al.* observed a great probability of facial bone fracture with a standard steering wheel loading above 1400 N [7]. Nyquist *et al.* performed horizontal guided impacts on facial bone of isolated heads [8]; and obtained a mean threshold for severe fracture of 3000 N. Even if these experiments include various loading conditions, all cases can not been studied experimentally due to the availability of post mortem human subjects. Moreover, the existing experiments are difficult to use as validation tests for finite element models since the protocols only offer global curves (force/displacement or acceleration/time) and since some boundary and loading conditions carried out, such as padding or neck effect, are difficult to simulate.

The finite element models offer the possibility to analyze the injury mechanisms in detail and to study the effects of impact conditions on these mechanisms. Existing finite element models of the head are commonly built using medical imaging [magnetic resonance imaging or computed tomography or compouted tomography (CT) scans] obtained from specific anatomical pieces or anatomical database such as Visible Human Project [9]–[14]. Reconstruction quality depends on image resolution and step slice. However, if these parameters are optimized, this acquisition method is very useful since all tissues can be extracted and internal surfaces are then accessible. Another acquisition method is the three-dimensional (3-D) measurement device which allows the location of points on the structure [15]–[18]. However the internal surface of skull and facial cavities are not accessible when using such a device.

Two meshing strategies are found in the literature: the first consists in a direct meshing whereas the second is based on a geometric reconstruction. Direct meshing can be performed from medical images and consists in converting each bone voxel of the imaged volume in a brick element [12]. However, this solution presents many disadvantages. First, the mesh obtained shows irregular boundaries in a "stair" shape. Next, the constant mesh density leads to a lack of elements in thin facial bones when voxel resolution is reasonable, and to an excessive number of elements on the whole model when resolution is higher. A direct meshing method can also use points picked out on the internal and external surface of skeleton and these points are connected to build brick elements [17], [18]. However, such mesh depends on the number of points and, thus, presents coarse density. Volume based on geometric reconstruction can be meshed with hexahedral or tetrahedral elements. However, these models present coarse density in order to minimize simulation time [9], [10] and they do not have enough elements in the thickness of the structure.

Surface meshes are constituted by four-nodeand three-nodeshells and present adapted mesh density [11], [15], [16]. However, two principal weaknesses are identified for this mesh type. First, this kind of element theoretically represents mean surface but this one is particularly difficult to build. Thus, the meshed surface is generally the internal or external one. Second, the principal weakness of shell meshes is that thickness must be evaluated and the models found in literature have a constant thickness across the whole structure.

Finite element head models found in literature have a limited field of application. The models used for injury risk prediction in crashworthiness [9], [10], [15], [16] do not represent facial bones accurately, since they mainly focus on the skull content. The head models devoted to medical applications [11], [12], [17], [18] represent realistic geometry, but their mesh is coarse and not adapted to dynamic simulation. Furthermore, with regard to experimental validation, few of these models are validated by comparison to the mechanical behavior of real anatomical element, and when they are, it is thanks to the data obtained from the experimental studies described above, where the boundary conditions are not accurately known. Thus, one can note the absence, in literature, of head models showing realistic facial geometry, non restrictive application fields and accurate validation.

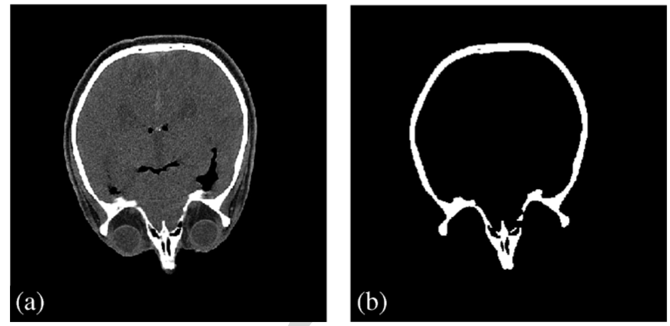

Fig. 1. Skull geometry acquisition. (a) Transverse CT scan at orbital level in headneck visualisation window. (b) Segmented corresponding image.

The work presented in this paper was conducted to realize a finite element model of the skull and face bones to be used in a wide field of applications. After finite element mesh completion, great care was taken in the experimental validation of this model. A static compression test was performed on the zygomatic bone, and displacement fields were measured using a digital image correlation technique. Local quantitative comparison of the model's behavior and response of anatomical element allowed the assessment of this finite element model.

II. Material and Methods

A. Finite Element Modeling of Skull and Facial Bones

An isolated fresh human head was used to obtain our model of skull and face. It came from an 80 year-old male donor, who was not affected by any pathology. After removing, this anatomical piece was stored at 4°C for a few days before processing.

Geometrical acquisition was realized at the radiology unit of Lyon Sud Hospital using a Siemens Somatom plus 4 scanner. Thickness, advance and reconstruction parameters were, respectively, 2, 3, and 1 mm in order to obtain a good resolution of the 3-D images of the head. CT scans were filtered during processing by a standard AB82 medical filter. A total of 199 slices were exported in DICOM format with a transversal resolution of 0.5 mm and a 512 $\times$ 512 pixel matrix.

Image segmentation consisted in the identification of bone material on the scan slices. For this purpose, images files were first converted into bmp standard format using eFilm Workstation shareware developed by Merge eFilm, which allows the use of several visualization windows. The window which showed the best contrast between bone and flesh tissues, and which presented a homogeneous aspect for bone material was the head neck window [Fig. 1(a)]. Then a shade adjustment, followed by a simple thresholding, performed with Paint shop Pro and Microsoft Photoeditor, permitted to isolate bone material on these pictures [Fig. 1(b)].

Once bone structure was isolated, the median surface of the head skeleton was built [Fig. 2(a)] using a program developed in our laboratory with the Visual Basic language. This program

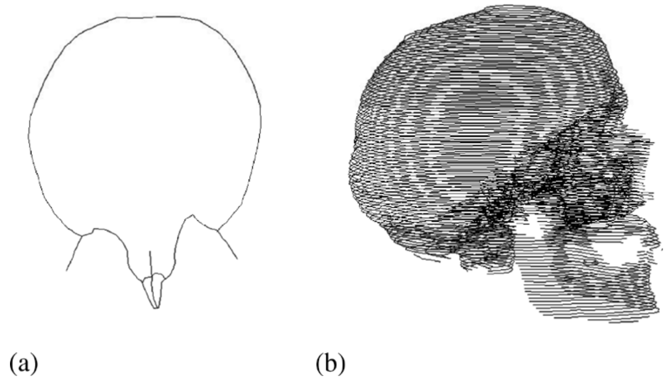

Fig. 2. Geometry reconstruction. (a) Mean outline example. (b) Whole head skeleton reconstruction.

allowed an automatic recognition of the skull bone median outline. A manual drawing was required for the median outline of the facial bones, which were complex and sometimes partially represented on CT scan. For example, nasal bones, whose thickness is inferior to the CT scan resolution, have been recognized and reconstructed manually with the help of an anatomist. Then, median outlines obtained on each slice were stacked [Fig. 2(b)] and written in a specific format used for CAD applications. Finally, the median surface of the bone structure was built using a CAD software (CATIA V4, Dassault Systèmes) by linking each segment forming a median outline to its neighboring counterpart by a curved surface.

The finite element mesh is constituted by shell elements lying on the median surface of the skull. The mesh density is variable in order to represent accurately the real geometry of the face and skull, with particularly small elements on complex structures of facial bones. In order to allow the simulation of the mechanical behavior by the finite element method, the quality of the elements was continuously checked during construction, using standard criteria like warp factor and distortion. The final mesh of the skull and the facial bones is composed of 4413 four-node and 270 three-node shell elements (Fig. 3). Elements' size varied from 1.5 mm^2, in order to finely represent the complex facial structure (Fig. 3), to 1.5 cm^2 on cranial part. Once the mesh was built, real thickness was assigned to each element, according to the following method. First, the element's four (or three) nodes were identified on the volume of binary images of bone structure. Then, the segments perpendicular to the element's surface, and going through these nodes, were created in the images volume. The voxels were covered along these segments in order to find the bone boundary. Then, the element's thickness was computed as the mean value of distances measured on its three or four nodes. The thickness of the shell elements, measured by this method, varied from 0.5 up to 19 mm and corresponded well to the anatomical structure of the head skeleton. The minimal values were located on maxilla sinuses, orbits and temporal bones whereas maximal values were found on the occipital protuberance. After the geometry acquisition, the modeled head was submitted to static compression test on zygoma bone in order to identify Young's modulus using numerical simulation. This study, already published, showed that the identified Young's modulus was 3700 MPa [19].

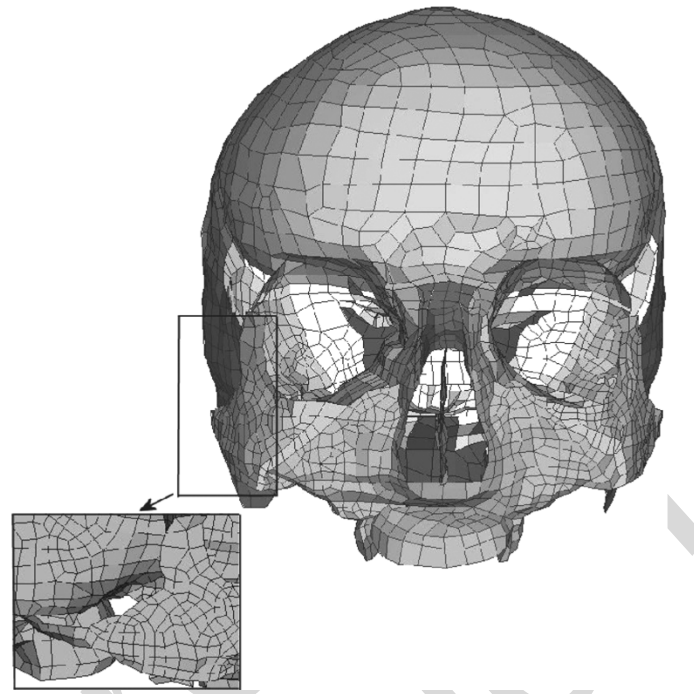

Fig. 3. Frontal view of the finite element model of head skeleton and lateral detailed view of the zygomatic arch.

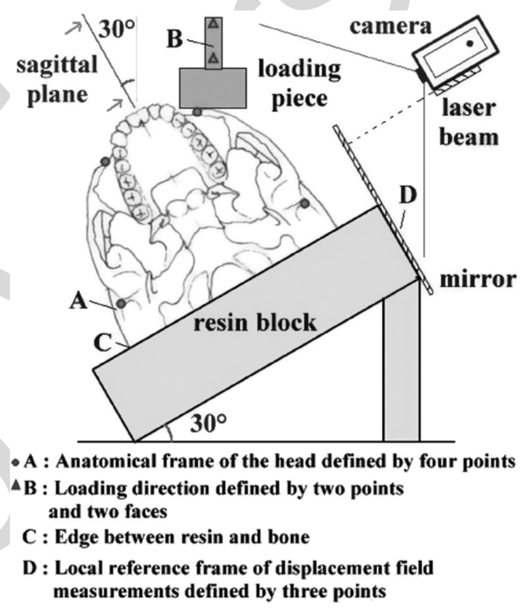

Fig. 4. Experimental configuration of compression test.

B. Tests and Measurements Protocol

A quasi-static compression test was performed on an anatomical piece which was removed from an 80-year-old female donor. Prior to testing, soft tissues were removed mechanically and the rear part of the skull was cut off in frontal plane behind the mastoids' process. The facial part obtained was cleaned in an oxygen water bath and conserved by freezing until mechanical testing. Finally, a physiologic bath re-hydrated it at ambient temperature during two days prior testing.

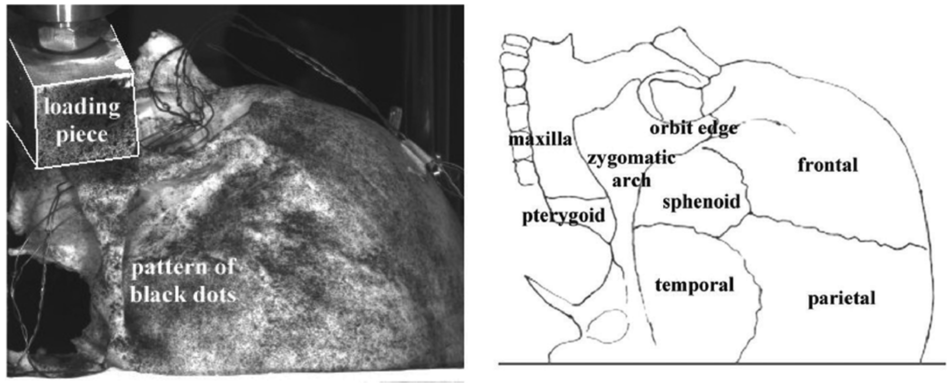

(a) (b)

Fig. 5. Two-dimensional deformation field measurement by digital correlation. (a) Image produced by the camera. (b) Separated view of skull structure shown on image.

The compressive load was applied to the facial bone structure by an universal Deltalab compression machine, with a displacement velocity of 0.5 mm/min. The loading was carried out up to rupture on left zygomatic bone with a 30° oriented direction to the sagittal plane (Fig. 4).

To ensure fixed boundary conditions, the rear part of the facial structure was embedded into a 240-mm-sided steel platform with a five centimeters TECKNOVIT3040 resin block ($E_{resin} = 2000\ \mathrm{MPa}$). This apparatus was screwed on the fixed horizontal platform of the loading machine, with the face viewing toward the top (Fig. 4). Thirty degrees orientation of facial part was ensured by three steel machined wedges. The loading piece was a parallelepiped with a contact surface of 12 cm^2.

The loading machine was equipped with a load cell (TME F521 TC) and a global displacement transducer to record force deflection curve. Two-dimensional (2-D) displacement fields of the loaded facial part were measured by digital image correlation [20], [21]. For that, a randomized pattern of black dots was realized by depositing carbon powder on the anatomical piece, previously coated with wood glue solution. During the compression test, topography of this pattern was recorded at initial and loaded state using a 1024 × 1024 pixels numerical camera (CDD Hamamatsu C4742-95) (Fig. 5).

Then, the correlation was performed between each pair of digital images (initial and loaded states) using ICASOFT software (Techlab, France) to determine displacement fields.

For the correlation calculations, the image of the measured area is divided into groups of square pixels called patterns, in which the displacement field is considered to be homogeneous. In such a theory, an image is defined by a discrete function of grey levels, of which the value varies from 0 to 255. In doing so, a discrete function $f(u, v)$ is attributed to the initial image representing the specimen before distortion. For the deformed image, the discrete function will be transformed to $f^*(u^*, v^*)$ (1) where $DU(u, v)$ and $DV(u, v)$ represent the 2 components of the displacement field for a pattern

$$f^*(u^*, v^*) = f^*(u + DU(u, v), v + DV(u, v). \qquad (1)$$

The mathematical definition of the displacement field on a pattern, including both strain and rigid body displacement terms is defined in (2) where du and dv are the rigid body translation terms, au, av, bu, and bv the elongation terms and cu and cv the shearing terms

$$\begin{cases} DU(u, v) = a_u \cdot u + b_u \cdot v + c_u \cdot u \cdot v + d_u \\ DV(u, v) = a_v \cdot u + b_v \cdot v + c_v \cdot u \cdot v + d_v \end{cases}. \qquad (2)$$

The purpose of the method is then to compare these two functions by computing a correlation coefficient (3), in order to find the final pattern which best matches the initial one. The corresponding f^* solution is obtained by minimisation of this correlation coefficient, where ΔM represents the surface of the pattern in the initial image

$$C_2 = 1 - \frac{\int_{\Delta M} f(u, v) \cdot f^*(u^*, v^*) \cdot du \cdot dv}{\sqrt{\int_{\Delta M} f(u, v)^2 \cdot du \cdot dv \cdot \int_{\Delta M} f^*(u^*, v^*)^2 \cdot du \cdot dv}}. \qquad (3)$$

Two-dimensional displacements were expressed in the local frame linked to digital images and formed by upper left corner, horizontal and vertical edges (Fig. 5). Picture plane was adjusted to be parallel to platform edge in which the anatomical piece is embedded, in order to give a lateral view of the head (Fig. 4). For this purpose, an adjustment of camera's direction was ensured by a mirror and a laser beam. The accuracy of the displacement measurement was equal to 0.05 mm. It was obtained by computing the displacement field of a mechanical part, which was supposed not to deform during loading.

C. Numerical Simulation and Response Assessment

Numerical simulation of the compression test described in the previous paragraph was performed using ABAQUS implicit code. In order to reproduce experimental boundary conditions during simulation, the location of particular points (Fig. 4) were recorded before tests using a 3-D measurement device FaroArm. These points defined: 1) the anatomical frame of the head, which is based on Frankfort's plane [22]; 2) the loading direction; 3) the edge formed by resin and bone; 4) the local reference frame for displacement field measurements. The anatomical frame of the head, also defined in the finite element model, constituted the transition frame from mechanical test to numerical simulation.

Then, the nodes forming the edge between bone and resin were fixed, and elements belonging to posterior part were removed. It was previously checked that these fixed boundary conditions were equivalent to the modeling of the resin block. The loading plate was finely meshed with rigid shell elements. Contact pair between bone elements and rigid body was modeled with a Coulomb friction coefficient equal to 0.3. In order to avoid contact problems due to the irregular shape of the loaded area, the four bone elements in contact with the rigid piece were given a particular rigidity ($\mathrm{E} = 300000\ \mathrm{MPa}$), so that they couldn't be deformed during loading.

Bone material was homogeneous, isotropic, with an elasto-plastic behavior defined by Young modulus E, yield stress $\sigma\mathrm{e}$, and tangent modulus E'. The Poisson coefficient ν was chosen equal to 0.21 [15], [23]. Young modulus E was defined by identification of linear part of numerical and experimental force versus displacement curves. Next, plastic properties $\sigma\mathrm{e}$ and E' were identified. In order to achieve the identification, a first simulation was carried out, using a perfectly plastic behavior law, a dichotomy method allowed the coincidence of curves to determine $\sigma\mathrm{e}$. Then, for the tangent modulus value, the same method allowed the adjustment of experimental curve with the numerical curve obtained using a plastic law, with E and $\sigma\mathrm{e}$ determined previously.

The local validation of the head's finite element model was carried out by comparing the local numerical response, obtained using the mechanical properties given above, to the displacement field experimentally measured by digital correlation. For a same load level equal to 1005 N, the displacements were decomposed between two directions defined by image's local frame. The results were first analyzed qualitatively with the displacements distribution over the head. Then, the local validation of the finite element model was analyzed quantitatively. In this way, the relative error between the displacements measured by digital image correlation and those computed by the finite element method was calculated as follows:

$$e_r = \frac{U_{\exp} - U_{sim}}{U_{\exp}}. \tag{4}$$

The relative error values were distributed over the finite element model with the aim to analyze results with their anatomical location.

III. Results

A. Mechanical Properties Identification

The best adjustment of the numerical force-displacement curve to fit the experimental one was obtained for the following elasto-plastic properties: $\mathrm{E} = 1600\ \mathrm{MPa}$, $\sigma\mathrm{e} = 5\ \mathrm{MPa}$, $\mathrm{E}' = 1400\ \mathrm{MPa}$ (Fig. 6).

B. Local Assessment of the Finite Element Model

The observation of the displacement distribution measured by correlation showed that the two-dimensional (2-D) movement

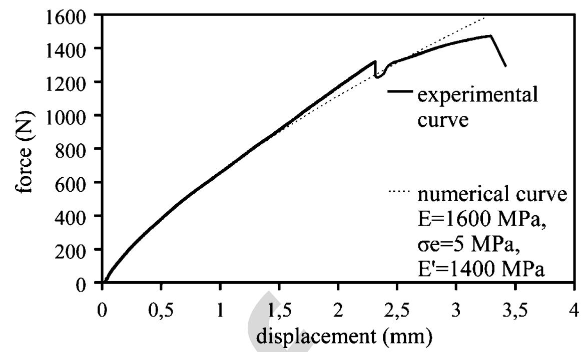

Fig. 6. Identification of bone material properties.

of the facial structure between the beginning of the test and the level load of 1005 N was an association of two structure displacements (Fig. 7).

- A translation in the vertical loading direction, which was maximal under the loading plate.
- A rotation, characterized by an horizontal displacement toward the vertex for the lower part of the face and toward the mandible for the upper part. A maximum value was observed for the thinner part of the zygomatic arch as well as for the sphenoid bone.

Two facial components acted as reinforcement pillars during the loading: the zygomatic arch which bent on its smaller section due to the loading orientation unaligned to the arch axis, and the orbital edge which was submitted to tensile loading. Then, limited forces were transmitted to the skull through the frontal and the sphenoid bones.

First, a qualitative comparison was made between experimental results and model's response. To obtain a clear representation of the experimental and numerical displacement distributions, scales were adjusted separately. The 2-D movements shown by the finite element model for this test simulation are similar to displacements of anatomical part described above: maximal values had the same location and displacement signs were equivalent [Fig. 7(c) and (d)]. However, for the horizontal direction, the maximal displacement located on zygomatic arch was larger in the numerical simulation.

Quantitatively, the experimentally measured horizontal displacements ranged from -0.06 to 0.06 mm. These values were too small to be analyzed accurately since they were approaching the measurement accuracy and then the relative error was not calculated for this measurement direction. The experimentally measured vertical displacements varied between 0.14 mm on skull to 0.47 mm on zygomatic bone. The minimal value was high considering its location which was far from the loading plate and near the fixed boundary conditions. The vertical displacements computed using the finite element model had a larger range from -0.1 mm on skull to 0.9 mm on zygomatic bone. The relative error of vertical displacements varied between 8% on the lower part of the zygomatic arch to 70% on the upper part of zygomatic arch (Fig. 8). The minimal error of 8% is obtained for measured and computed vertical displacements, respectively, equal to 0.25 mm and 0.229 mm. The relative

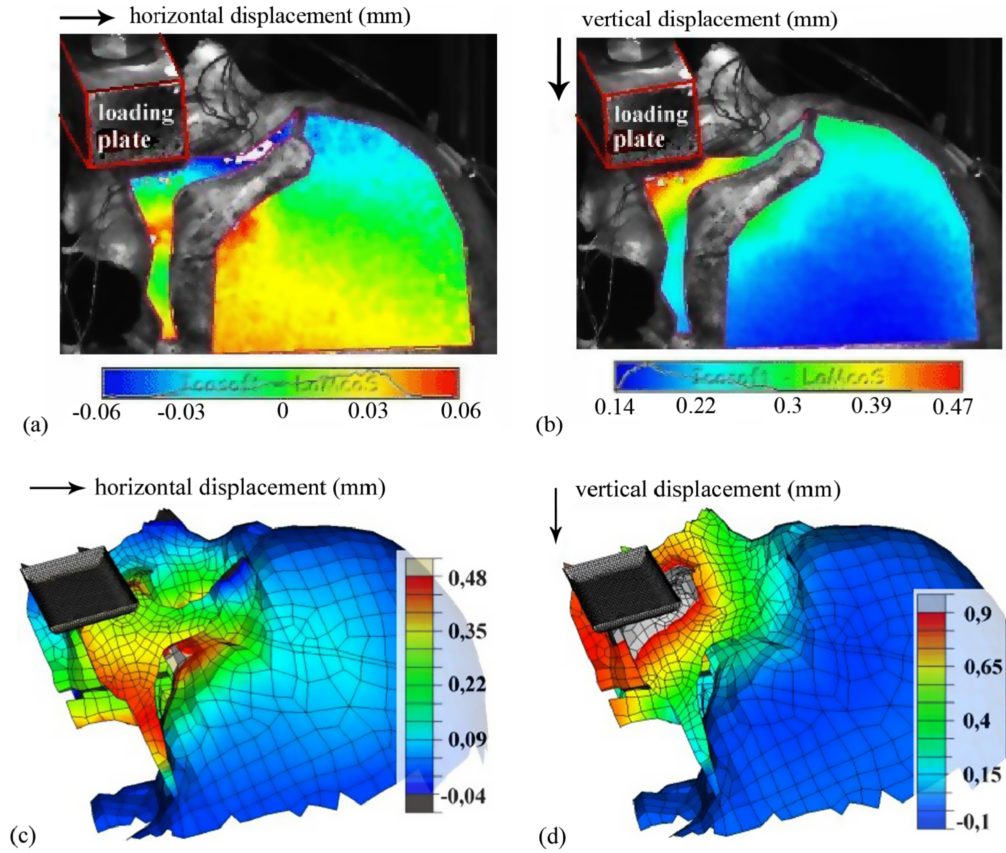

Fig. 7. Measured and computed 2-D displacements of the lateral part of the head skeleton. (a) Distribution of horizontal displacements on anatomical part. (b) Distribution of vertical displacements on anatomical part. (c) Distribution of horizontal displacements on model. (d) Distribution of vertical displacements on model. (Color version available online at http://ieeexplore.ieee.org.)

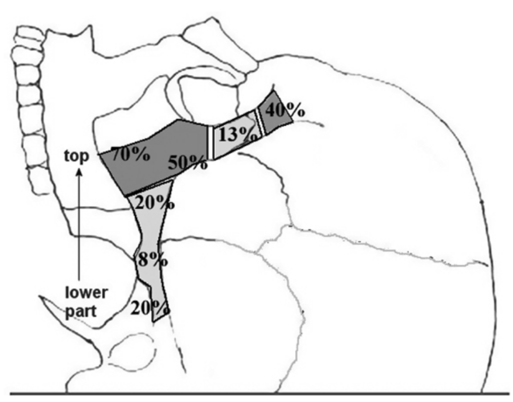

(a)

position	Usim (mm)	Uexp (mm)	er (%)
lower part	0.148427	0.231	35.74
	0.181027	0.239	24.25
	0.209653	0.2489	15.76
	0.229181	0.25	8.32
	0.277674	0.245	-13.33
	0.288677	0.26	-11.03
	0.417896	0.324	-28.98
	0.397703	0.279	-42.54
	0.397301	0.329	-20.76
	0.653078	0.39	-67.45
	0.611181	0.377	-62.11
	0.536483	0.359	-49.43
	0.778555	0.46	-69.25
	0.735418	0.431	-70.63
	0.68432	0.41	-66.9
top	0.639913	0.395	-62

(b)

Fig. 8. Distribution of the relative error for computed vertical displacement of the lateral part of the head skeleton. (a) Schema of the distribution. (b) Summary table.

error of 70% corresponds to measured and computed values of 0.43 mm and 0.73 mm, respectively.

IV. Discussion and Conclusion

The finite element model of the human head skeleton presented in this paper is based on an accurate geometric reconstruction performed using CT scan slices. The fine scan resolution and step slice, as well as the variable density of the mesh allowed a good accuracy of the bone structure representation. Moreover, since thickness is an important parameter in structure behavior under loading, the allocation of real thickness to elements ensures more accuracy in mechanical behavior simulation. In view of using the model for dynamical simulations as well as for static computation, a particular care was taken to avoid the use of three nodes elements and to limit the number of elements for a reasonable computational time.

The loading location and direction chosen for static compression tests is compatible with a realistic car crash situation.

The 30° oriented loading on zygomatic bone corresponds to the impact conditions of face on the steering wheel when the car does not have an air bag and the driver wears his seat belt. The first rupture of bone structure occurred for a force value equal to 1319 N which is close to those given by Allsop (1737.5 N) for impact tests with fixed boundary conditions [6]. The quite large range observed in rupture values is linked to the test conditions (boundaries, static or dynamic test, velocity) and to the anatomical part characteristics such as morphology, age and gender of the subject, absence of soft tissues. The values for the mechanical parameters obtained by identification from the experimental curve are the elasto-plastic properties of the whole bone structure ($\mathrm{E} = 1600$ MPa, $\sigma\mathrm{e} = 5$ MPa, and $\mathrm{E}' = 1400$ MPa).When comparing these values to literature on mechanical properties of cranial bone, they correspond to minimal values of interval given by Delille [24], who performed bending tests and identification of elasto-plastic properties on 67 samples coming from 12 subjects. The Young's modulus is also in the range of values obtained by McElhaney *et al.* [23].

The model's behavior was compared to the displacement field measurements obtained using a digital image correlation technique. Qualitatively, the displacement distribution simulated with the model is very similar to the real one, even if the maximum value of the zygomatic arch's horizontal displacement is more localized in the experiment than in the simulation. This is due to the difference in zygomatic arch morphology since the tested and modeled head do not watch exactly. In fact, the narrower part of the real zygomatic arch shows the maximum horizontal displacement value because of bending movement. On the model the shape of the arch does not include this narrow section. Quantitatively, the measured and computed vertical displacements were close on the zygomatic arch and on the orbit edge. A large error is found on the skull and the upper part of the zygomatic bone. Several phenomena explain these results for the quantitative comparison. First, the experimental displacements measured on this area are subjected to limitations. The displacement field obtained using the digital image correlation technique was measured in a plane which was chosen parallel to the zygomatic arch. The orbit edge is also parallel to this plane whereas the cranial part and the upper area of the zygomatic bone are out of plane. Thus, external plane displacements may disturb the experimental measurements and the local comparison in these two areas. Moreover, the displacements measured are small and sometimes they are close to the measurement accuracy, as those located on the skull, near the fixed boundary conditions. Second, as we saw for the qualitative comparison, the structure geometry is an important factor which introduces some bias in local comparison between anatomical part and model's behavior. In fact, the geometrical variability is high between one subject and another; this may disturb the mechanical response as well as the location of boundary and loading conditions.

This new measurement technique adapted to anatomical part of the body presents some limitations due to the specificity of the tested object. Nevertheless, on an appropriate measurement area, it brings important information that shows first a good qualitative correspondence, and second a small relative error equal to 8% between anatomical part and finite element model. Thus, this comparison allows the validation of our finite element model of the human head skeleton.

In the literature, the assessment of models of the head bone structure is usually based on the comparison of global curves (force/displacement or acceleration/time) since local data are not easy to acquire. Moreover, boundary and loading conditions of some experiments used for validation are not described accurately (padding, neck effect, etc.) and are difficult to simulate.

The new assessment method presented in this paper contributes to improve the validation of finite element model since it is divided into two steps: the adjustment of numerical to experimental data measured on the loading point which is commonly used, and then a local validation performed using a digital correlation method on a large area of the structure. Further investigations will be carried out to adapt the digital correlation technique to 3-D measurements and to dynamical loading. Our finite element model of human head skeleton was validated using this assessment method under static loading and is now available for a large field of applications.

ACKNOWLEDGMENT

The authors would like to thank P. Clerc (Mecanium SARL) for the realisation of digital correlation measurements, P. Lapellerie for his contribution to the PMHS experiments, and Dr. F. Cotton for the CT scan.

REFERENCES

[1] F. Roccia, F. Servadio, and G. Gerbino, "Maxillofacial fractures following air bag deployment," *J. Cranio-Maxillofacial Surg.*, vol. 27, pp. 335–338, 1999.

[2] K. Hussain, D. B. Wijetunge, S. Grubnic, and I. T. Jackson, "A comprehensive analysis of craniofacial trauma," *J. Trauma*, vol. 36, no. 1, pp. 34–46, 1994.

[3] Association for the Advancement of Automotive Medicine, Barrington, IL, The Abbreviate Injury Scale, Update 98 1998.

[4] B. Laumon, Recherches coordonnées sur les traumatismes consécutifs à un accident de la circulation routière, et sur leurs causes et conséquences 0206, 2002, p. 292, 129.

[5] A. M. Nahum, J. D. Gatts, C. W. Gadd, and J. Danforth, "Impact tolerance of the skull and face," in *Proc. 12th Stapp Car Crash Conf.*, Detroit, MI, 1968, pp. 302–316.

[6] D. L. Allsop, C. Y. Warner, M. G. Wille, D. C. Schneider, and A. M. Nahum, "Facial impact response- a comparison of the hybrid III dummy and human cadaver," in *Proc. 32nd Stapp Car Crash Conf.*, Atlanta, GA, 1988, pp. 139–155.

[7] N. Yoganandan, A. Sances, F. A. Pintar, D. J. Maiman, D. C. Hemmy, S. J. Larson, and V. M. Haughton, "Traumatic facial injuries with steering wheel loading," *J. Trauma*, vol. 31, no. 5, pp. 699–710, 1991.

[8] G. W. Nyquist, J. M. Cavanaugh, S. J. Goldberg, and A. I. King, "Facial impact tolerance and response," presented at the Stapp Car Crash Conf., 1988, Paper 861896.

[9] M. Claessens, *Finite Element Modeling of the Human Head Under Impact Conditions*. Eindhoven, The Netherlands: Technishe Universiteit Eindhoven, 1997, p. 137.

[10] H. Y. Choi, S. H. Lee, I. H. Lee, and E. Haug, "Finite element modeling of human head-neck complex for crashworthiness simulation," in *Proc. Conf. Computational Fluid and Solid Mechanics*, 2001, pp. 114–119.

[11] H. Iseri, A. E. Tekkaya, O. Ostan, and S. Bigic, "Biomechanical effects of rapid maxillary expansion on the craniofacial skeleton, studied by the finite element method," *Eur. J. Orthodont.*, vol. 20, pp. 347–356, 1998.

[12] U. Hartmann, F. Kruggel, T. Hierl, G. Lonsdale, and R. Klöppel, "Skull mechanic simulations with the prototype SimBio environment," in *Proc. Conf. Computational Fluid and Solid Mechanics*, 2001, pp. 243–246.

[13] T. J. Horgan and M. D. Gilchrist, "The creation of three-dimensional finite element models for simulating head impact biomechanics," *Int. J. Crashworthiness*, vol. 8, no. 4, pp. 353–366, 2003.

[14] L. Zhang, K. H. Yang, R. Dwarampudi, K. Omori, T. Li, K. Chang, W. N. Hardy, T. B. Khalil, and A. I. King, "Recent advances in brain injury research: a new human head model development and validation," *Stapp Car Crash J.*, vol. 45, pp. 369–393, 2001.

[15] Kang, R. Willinger, and B. M. Diaw, "Validation of a 3D anatomic human head model and replication of head impact in motorcycle accident by finite element modeling," presented at the 41st Stapp Car Crash Conf., 1997.

[16] R. Willinger, B. M. Diaw, and H. S. Kang, "Finite element modelling of skull fractures caused by direct impact," *Int. J. Crashworthiness*, vol. 5, no. 3, pp. 249–258, 2000.

[17] K. Tanne, S. Matsubara, and M. Sakuda, "Location of the centre of resistance for the nasomaxillary complex studied in a three-dimensional finite element model," *Br. J. Orthod.*, vol. 22, no. 3, pp. 227–232, 1995.

[18] H. Jinushi, T. Suzuki, T. Naruse, and Y. Isshiki, "A dynamic study of the effect on the maxillofacial complex of the face bow: analysis by a three-dimensional finite element method," *Bull. Tokyo Dent. Coll.*, vol. 38, no. 1, pp. 33–41, 1997.

[19] B. Autuori, K. Bruyère-Garnier, F. Morestin, M. Brunet, and J. P. Verriest, "Assessment of a finite element model of the human facial bone structure," in *27e Congrès de la Société de Biomécanique*, Valenciennes, France, Sep. 2002, vol. 110, Archives of physiology and biochemistry, p. 36.

[20] S. Mguil-Touchal, F. Morestin, and M. Brunet, "Various experimental applications of digital image correlation method," in *Proc. CMEM 97*, 1997, pp. 45–58.

[21] P. Clerc, F. Morestin, and M. Brunet, "Measurement of deformation fields using numerical images correlation," in *Proc. AMPT'99 IMC16*, 1999, vol. 3, pp. 1889–1897.

[22] K. Bruyere, F. Bermond, R. Bouquet, Y. Caire, M. Ramet, and E. Voiglio, "Human Maxilla bone response to 30 ° oriented impacts and comparison with frontal bone impacts," presented at the 44th Association for the Advancement of Automotive Medicine (AAAM) Conf., , Chicago, IL, Oct. 2–4, 2000.

[23] J. H. McElhaney, J. L. Fogle, J. W. Melvin, R. R. Haynes, V. L. Roberts, and N. M. Alem, "Mechanical properties of cranial bone," *J. Biomech.*, vol. 3, pp. 495–511, 1970.

[24] C. Dellile, "Contribution à l'identification de lois matérielles de l'os du crâne humain en quasi-statique à partir d'expérimentations et de simulations numériques," in *Génie Mécanique*. Valenciennes, France: Université de Valenciennes et du Haut Cambrésis, 2002, p. 190.

Barbara Autuori received the Ph.D. degree for the development of a finite element model on the human facial skeleton, from INSA, Lyon, France, in April 2004.

She was involved in the Science and Technology in the Transport Safety (ST2) project as a Postdoctoral Researcher at the Laboratory of Industrial and Human Automation, Mechanics and Computer Science, Valenciennes, France. Her job was to evaluate the injury risk of car drivers in precrash situation.

Karine Bruyère-Garnier Please provide biographical information (and photo if available).

Fabrice Morestin Please provide biographical information (and photo if available).

Michel Brunet Please provide biographical information (and photo if available).

Jean-Pierre Verriest Please provide biographical information (and photo if available).

Finite Element Modeling of the Head Skeleton With a New Local Quantitative Assessment Approach

Barbara Autuori*, Karine Bruyère-Garnier, Fabrice Morestin, Michel Brunet, and Jean-Pierre Verriest

***Abstract*—The present study was undertaken to build a finite element model of the head skeleton and to perform a new assessment approach in order to validate it. The application fields for such an improved model are injury risk prediction as well as surgical planning. The geometrical reconstruction was performed using computed tomography scans and a total of 4680 shell elements were meshed on the median surface of the head skeleton with the particular characteristic of adapted mesh density and real element thickness. The assessment protocol of the finite element model was achieved using a quasi-static experimental compression test performed on the zygomatic bone area of a defleshed isolated head. Mechanical behavior of the finite element model was compared to the real one and the assessment approach was divided into two steps. First, the mechanical properties of the anatomical structure were identified using the simulation and then the simulated displacement field was compared to local displacement measurement performed during test using a digital correlation method. The assessment showed that the head skeleton model behaved qualitatively like the real structure. Quantitatively, the local relative error varied from 8% up to 70%.**

***Index Terms*—Biomechanics, compressive tests, finite element modeling, skull.**

I. Introduction

THE head skeleton is a complex structure whose specific architecture ensures the protection of cranial contents and sense organs. The principal causes of facial injuries are road accidents, falls, fight and sports activities [1]. Facial fractures observed in medical services concern mainly the nose, skull, mandible, zygomatic, and bones, and more rarely, orbits and maxilla [2]. In terms of threat to life [3], facial wounds are minor [4] whereas skull and brain injuries are severe and can be fatal to victims. This explains that skull fractures and brain injuries are commonly studied using experimentation or, more recently, by computational method whereas facial injuries are not.

Finite element modeling is a numerical method which allows for the reproduction of a particular loading on a structure, with varying parameters. Moreover, local mechanical parameters useful for phenomena characterization can be computed. For example, stress, as well as strain, is given by finite element models, whereas they can not easily be measured experimentally. The scope of applications for these finite element models of human body segments appears extremely wide; for the head they concern the following.

- Better understanding of injury mechanisms and pathological dysfunction.
- Injury risk prevention and protection, such as protection systems testing for road users (helmets), or fracture prevention of repaired bones.
- Surgical planning, such as in maxillofacial surgery cases which require force applications and bone displacements.

One may wonder if facial bone studies present much interest, considering the minor severity of facial injury when compared with brain injuries. Many arguments can be put forward to address this issue. First, in spite of their low life-threatening potential, facial fractures need several surgical acts to be repaired and they leave aesthetic as well as psychological sequels. Moreover, nowadays patients do not hesitate to resort to surgery in order to repair pathologic abnormalities or aesthetic traits, since aesthetic surgery has become common. Second, in view of injury prevention, finite element models of the head should have a realistic face, in order for brain injuries to be correctly predicted in the case of face impact. This is why facial bone modeling presents much relevance in various applications such as head injury prediction or surgical planning.

The facial bones have been experimentally studied by several authors, mainly in order to determine their tolerance to impact. For a particular bone tested, results found in these studies depend on experimental conditions. For drop tests on zygomatic bone, performed with plane contact surface, Nahum [5] found impact force tolerances equal to 890 N. When the head is isolated from the body and more rigidly fixed during impact, the force measured is slightly higher than the figures given above. Thus, force threshold for zygomatic bone found by Allsop [6] is 1737.5 N and Yoganandan *et al.* observed a great probability of facial bone fracture with a standard steering wheel loading above 1400 N [7]. Nyquist *et al.* performed horizontal guided impacts on facial bone of isolated heads [8]; and obtained a mean threshold for severe fracture of 3000 N. Even if these experiments include various loading conditions, all cases can not been studied experimentally due to the availability of post mortem human subjects. Moreover, the existing experiments are

Manuscript received August 12, 2004; revised September 25, 2005. This work was supported in part by the Medical Research Foundation. *Asterisk indicates corresponding author.*

*B. Autuori is with the Laboratory of Biomechanics and Human Modelling, INRETS of Bron, 25 Av. F. Mitterrand, case24, 69675 Bron Cedex, France (e-mail: barbara_autuori@yahoo.fr).

K. Bruyère-Garnier and J. P. Verriest are with the Laboratory of Biomechanics and Human Modelling, INRETS of Bron, 69675 Bron Cedex, France (e-mail: karine.bruyere@inrets.fr; jpv@inrets.fr).

F. Morestin and M. Brunet are with the Contact and Solid Mechanics Laboratory, INSA of Lyon, 69621 Villeurbanne Cedex, France (e-mail: Fabrice.Morestin@insa-lyon.fr; michel.brunet@insa-lyon.fr).

Digital Object Identifier 10.1109/TBME.2006.872812

difficult to use as validation tests for finite element models since the protocols only offer global curves (force/displacement or acceleration/time) and since some boundary and loading conditions carried out, such as padding or neck effect, are difficult to simulate.

The finite element models offer the possibility to analyze the injury mechanisms in detail and to study the effects of impact conditions on these mechanisms. Existing finite element models of the head are commonly built using medical imaging [magnetic resonance imaging or computed tomography or compouted tomography (CT) scans] obtained from specific anatomical pieces or anatomical database such as Visible Human Project [9]–[14]. Reconstruction quality depends on image resolution and step slice. However, if these parameters are optimized, this acquisition method is very useful since all tissues can be extracted and internal surfaces are then accessible. Another acquisition method is the three-dimensional (3-D) measurement device which allows the location of points on the structure [15]–[18]. However the internal surface of skull and facial cavities are not accessible when using such a device.

Two meshing strategies are found in the literature: the first consists in a direct meshing whereas the second is based on a geometric reconstruction. Direct meshing can be performed from medical images and consists in converting each bone voxel of the imaged volume in a brick element [12]. However, this solution presents many disadvantages. First, the mesh obtained shows irregular boundaries in a "stair" shape. Next, the constant mesh density leads to a lack of elements in thin facial bones when voxel resolution is reasonable, and to an excessive number of elements on the whole model when resolution is higher. A direct meshing method can also use points picked out on the internal and external surface of skeleton and these points are connected to build brick elements [17], [18]. However, such mesh depends on the number of points and, thus, presents coarse density. Volume based on geometric reconstruction can be meshed with hexahedral or tetrahedral elements. However, these models present coarse density in order to minimize simulation time [9], [10] and they do not have enough elements in the thickness of the structure.

Surface meshes are constituted by four-nodeand three-nodeshells and present adapted mesh density [11], [15], [16]. However, two principal weaknesses are identified for this mesh type. First, this kind of element theoretically represents mean surface but this one is particularly difficult to build. Thus, the meshed surface is generally the internal or external one. Second, the principal weakness of shell meshes is that thickness must be evaluated and the models found in literature have a constant thickness across the whole structure.

Finite element head models found in literature have a limited field of application. The models used for injury risk prediction in crashworthiness [9], [10], [15], [16] do not represent facial bones accurately, since they mainly focus on the skull content. The head models devoted to medical applications [11], [12], [17], [18] represent realistic geometry, but their mesh is coarse and not adapted to dynamic simulation. Furthermore, with regard to experimental validation, few of these models are validated by comparison to the mechanical behavior of real anatomical element, and when they are, it is thanks to the data obtained from the experimental studies described above, where the boundary conditions are not accurately known. Thus, one can note the absence, in literature, of head models showing realistic facial geometry, non restrictive application fields and accurate validation.

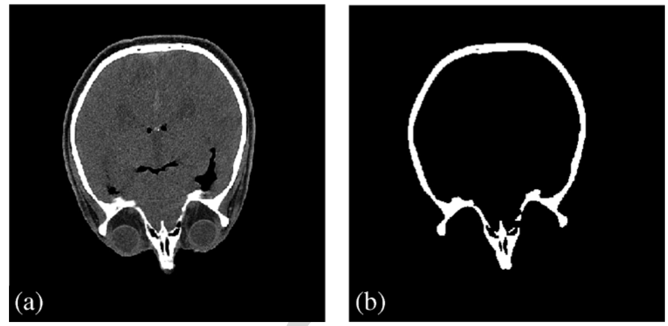

Fig. 1. Skull geometry acquisition. (a) Transverse CT scan at orbital level in headneck visualisation window. (b) Segmented corresponding image.

The work presented in this paper was conducted to realize a finite element model of the skull and face bones to be used in a wide field of applications. After finite element mesh completion, great care was taken in the experimental validation of this model. A static compression test was performed on the zygomatic bone, and displacement fields were measured using a digital image correlation technique. Local quantitative comparison of the model's behavior and response of anatomical element allowed the assessment of this finite element model.

II. Material and Methods

A. Finite Element Modeling of Skull and Facial Bones

An isolated fresh human head was used to obtain our model of skull and face. It came from an 80 year-old male donor, who was not affected by any pathology. After removing, this anatomical piece was stored at 4°C for a few days before processing.

Geometrical acquisition was realized at the radiology unit of Lyon Sud Hospital using a Siemens Somatom plus 4 scanner. Thickness, advance and reconstruction parameters were, respectively, 2, 3, and 1 mm in order to obtain a good resolution of the 3-D images of the head. CT scans were filtered during processing by a standard AB82 medical filter. A total of 199 slices were exported in DICOM format with a transversal resolution of 0.5 mm and a 512 × 512 pixel matrix.

Image segmentation consisted in the identification of bone material on the scan slices. For this purpose, images files were first converted into bmp standard format using eFilm Workstation shareware developed by Merge eFilm, which allows the use of several visualization windows. The window which showed the best contrast between bone and flesh tissues, and which presented a homogeneous aspect for bone material was the head neck window [Fig. 1(a)]. Then a shade adjustment, followed by a simple thresholding, performed with Paint shop Pro and Microsoft Photoeditor, permitted to isolate bone material on these pictures [Fig. 1(b)].

Once bone structure was isolated, the median surface of the head skeleton was built [Fig. 2(a)] using a program developed in our laboratory with the Visual Basic language. This program

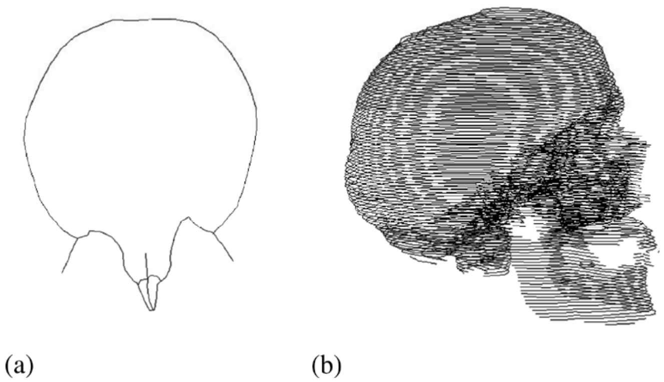

Fig. 2. Geometry reconstruction. (a) Mean outline example. (b) Whole head skeleton reconstruction.

allowed an automatic recognition of the skull bone median outline. A manual drawing was required for the median outline of the facial bones, which were complex and sometimes partially represented on CT scan. For example, nasal bones, whose thickness is inferior to the CT scan resolution, have been recognized and reconstructed manually with the help of an anatomist. Then, median outlines obtained on each slice were stacked [Fig. 2(b)] and written in a specific format used for CAD applications. Finally, the median surface of the bone structure was built using a CAD software (CATIA V4, Dassault Systèmes) by linking each segment forming a median outline to its neighboring counterpart by a curved surface.

The finite element mesh is constituted by shell elements lying on the median surface of the skull. The mesh density is variable in order to represent accurately the real geometry of the face and skull, with particularly small elements on complex structures of facial bones. In order to allow the simulation of the mechanical behavior by the finite element method, the quality of the elements was continuously checked during construction, using standard criteria like warp factor and distortion. The final mesh of the skull and the facial bones is composed of 4413 four-node and 270 three-node shell elements (Fig. 3). Elements' size varied from 1.5 mm^2, in order to finely represent the complex facial structure (Fig. 3), to 1.5 cm^2 on cranial part. Once the mesh was built, real thickness was assigned to each element, according to the following method. First, the element's four (or three) nodes were identified on the volume of binary images of bone structure. Then, the segments perpendicular to the element's surface, and going through these nodes, were created in the images volume. The voxels were covered along these segments in order to find the bone boundary. Then, the element's thickness was computed as the mean value of distances measured on its three or four nodes. The thickness of the shell elements, measured by this method, varied from 0.5 up to 19 mm and corresponded well to the anatomical structure of the head skeleton. The minimal values were located on maxilla sinuses, orbits and temporal bones whereas maximal values were found on the occipital protuberance. After the geometry acquisition, the modeled head was submitted to static compression test on zygoma bone in order to identify Young's modulus using numerical simulation. This study, already published, showed that the identified Young's modulus was 3700 MPa [19].

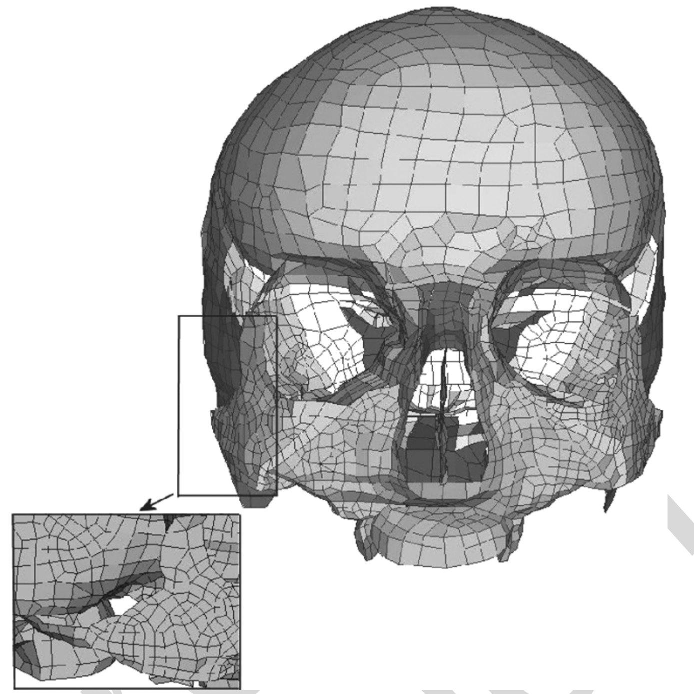

Fig. 3. Frontal view of the finite element model of head skeleton and lateral detailed view of the zygomatic arch.

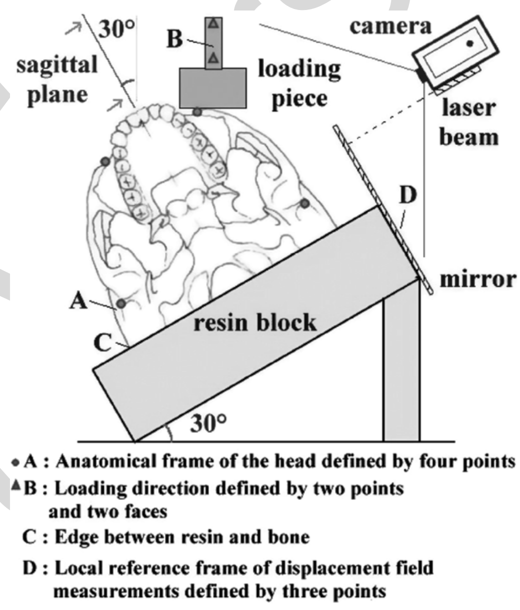

Fig. 4. Experimental configuration of compression test.

B. Tests and Measurements Protocol

A quasi-static compression test was performed on an anatomical piece which was removed from an 80-year-old female donor. Prior to testing, soft tissues were removed mechanically and the rear part of the skull was cut off in frontal plane behind the mastoids' process. The facial part obtained was cleaned in an oxygen water bath and conserved by freezing until mechanical testing. Finally, a physiologic bath re-hydrated it at ambient temperature during two days prior testing.

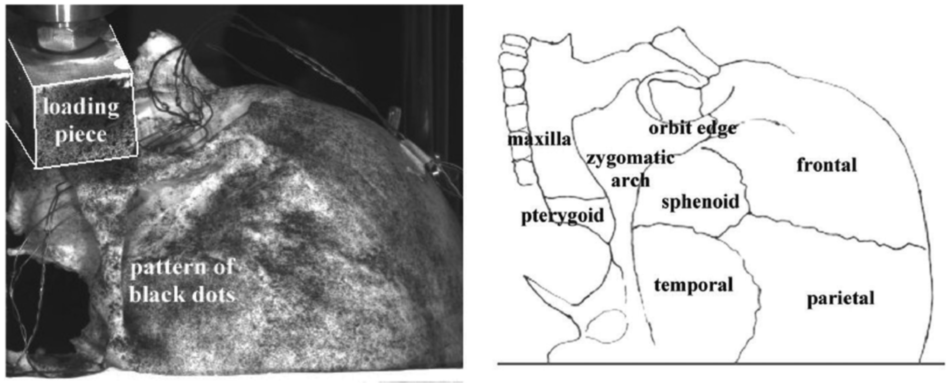

(a) (b)

Fig. 5. Two-dimensional deformation field measurement by digital correlation. (a) Image produced by the camera. (b) Separated view of skull structure shown on image.

The compressive load was applied to the facial bone structure by an universal Deltalab compression machine, with a displacement velocity of 0.5 mm/min. The loading was carried out up to rupture on left zygomatic bone with a 30° oriented direction to the sagittal plane (Fig. 4).

To ensure fixed boundary conditions, the rear part of the facial structure was embedded into a 240-mm-sided steel platform with a five centimeters TECKNOVIT3040 resin block ($E_{\mathrm{resin}} = 2000\ \mathrm{MPa}$). This apparatus was screwed on the fixed horizontal platform of the loading machine, with the face viewing toward the top (Fig. 4). Thirty degrees orientation of facial part was ensured by three steel machined wedges. The loading piece was a parallelepiped with a contact surface of 12 cm^2.

The loading machine was equipped with a load cell (TME F521 TC) and a global displacement transducer to record force deflection curve. Two-dimensional (2-D) displacement fields of the loaded facial part were measured by digital image correlation [20], [21]. For that, a randomized pattern of black dots was realized by depositing carbon powder on the anatomical piece, previously coated with wood glue solution. During the compression test, topography of this pattern was recorded at initial and loaded state using a 1024 × 1024 pixels numerical camera (CDD Hamamatsu C4742-95) (Fig. 5).

Then, the correlation was performed between each pair of digital images (initial and loaded states) using ICASOFT software (Techlab, France) to determine displacement fields.

For the correlation calculations, the image of the measured area is divided into groups of square pixels called patterns, in which the displacement field is considered to be homogeneous. In such a theory, an image is defined by a discrete function of grey levels, of which the value varies from 0 to 255. In doing so, a discrete function $f(u,v)$ is attributed to the initial image representing the specimen before distortion. For the deformed image, the discrete function will be transformed to $f^*(u^*,v^*)$ (1) where $DU(u,v)$ and $DV(u,v)$ represent the 2 components of the displacement field for a pattern

$$f^*(u^*,v^*) = f^*(u + DU(u,v), v + DV(u,v). \tag{1}$$

The mathematical definition of the displacement field on a pattern, including both strain and rigid body displacement terms is defined in (2) where du and dv are the rigid body translation terms, au, av, bu, and bv the elongation terms and cu and cv the shearing terms

$$\begin{cases} DU(u,v) = a_u \cdot u + b_u \cdot v + c_u \cdot u \cdot v + d_u \\ DV(u,v) = a_v \cdot u + b_v \cdot v + c_v \cdot u \cdot v + d_v \end{cases}. \tag{2}$$

The purpose of the method is then to compare these two functions by computing a correlation coefficient (3), in order to find the final pattern which best matches the initial one. The corresponding f^* solution is obtained by minimisation of this correlation coefficient, where ΔM represents the surface of the pattern in the initial image

$$C_2 = 1 - \frac{\int\limits_{\Delta M} f(u,v) \cdot f^*(u^*,v^*) \cdot du \cdot dv}{\sqrt{\int\limits_{\Delta M} f(u,v)^2 \cdot du \cdot dv \cdot \int\limits_{\Delta M} f^*(u^*,v^*)^2 \cdot du \cdot dv}}. \tag{3}$$

Two-dimensional displacements were expressed in the local frame linked to digital images and formed by upper left corner, horizontal and vertical edges (Fig. 5). Picture plane was adjusted to be parallel to platform edge in which the anatomical piece is embedded, in order to give a lateral view of the head (Fig. 4). For this purpose, an adjustment of camera's direction was ensured by a mirror and a laser beam. The accuracy of the displacement measurement was equal to 0.05 mm. It was obtained by computing the displacement field of a mechanical part, which was supposed not to deform during loading.

C. Numerical Simulation and Response Assessment

Numerical simulation of the compression test described in the previous paragraph was performed using ABAQUS implicit code. In order to reproduce experimental boundary conditions during simulation, the location of particular points (Fig. 4) were recorded before tests using a 3-D measurement device FaroArm. These points defined: 1) the anatomical frame of the head, which is based on Frankfort's plane [22]; 2) the loading direction; 3) the edge formed by resin and bone; 4) the local reference frame for displacement field measurements. The anatomical frame of the head, also defined in the finite element model, constituted the transition frame from mechanical test to numerical simulation.

Then, the nodes forming the edge between bone and resin were fixed, and elements belonging to posterior part were removed. It was previously checked that these fixed boundary conditions were equivalent to the modeling of the resin block. The loading plate was finely meshed with rigid shell elements. Contact pair between bone elements and rigid body was modeled with a Coulomb friction coefficient equal to 0.3. In order to avoid contact problems due to the irregular shape of the loaded area, the four bone elements in contact with the rigid piece were given a particular rigidity ($\mathrm{E} = 300000$ MPa), so that they couldn't be deformed during loading.

Bone material was homogeneous, isotropic, with an elasto-plastic behavior defined by Young modulus E, yield stress $\sigma\mathrm{e}$, and tangent modulus E'. The Poisson coefficient ν was chosen equal to 0.21 [15], [23]. Young modulus E was defined by identification of linear part of numerical and experimental force versus displacement curves. Next, plastic properties $\sigma\mathrm{e}$ and E' were identified. In order to achieve the identification, a first simulation was carried out, using a perfectly plastic behavior law, a dichotomy method allowed the coincidence of curves to determine $\sigma\mathrm{e}$. Then, for the tangent modulus value, the same method allowed the adjustment of experimental curve with the numerical curve obtained using a plastic law, with E and $\sigma\mathrm{e}$ determined previously.

The local validation of the head's finite element model was carried out by comparing the local numerical response, obtained using the mechanical properties given above, to the displacement field experimentally measured by digital correlation. For a same load level equal to 1005 N, the displacements were decomposed between two directions defined by image's local frame. The results were first analyzed qualitatively with the displacements distribution over the head. Then, the local validation of the finite element model was analyzed quantitatively. In this way, the relative error between the displacements measured by digital image correlation and those computed by the finite element method was calculated as follows:

$$e_r = \frac{U_{\exp} - U_{sim}}{U_{\exp}}. \tag{4}$$

The relative error values were distributed over the finite element model with the aim to analyze results with their anatomical location.

III. Results

A. Mechanical Properties Identification

The best adjustment of the numerical force-displacement curve to fit the experimental one was obtained for the following elasto-plastic properties: $\mathrm{E} = 1600$ MPa, $\sigma\mathrm{e} = 5$ MPa, $\mathrm{E}' = 1400$ MPa (Fig. 6).

B. Local Assessment of the Finite Element Model

The observation of the displacement distribution measured by correlation showed that the two-dimensional (2-D) movement

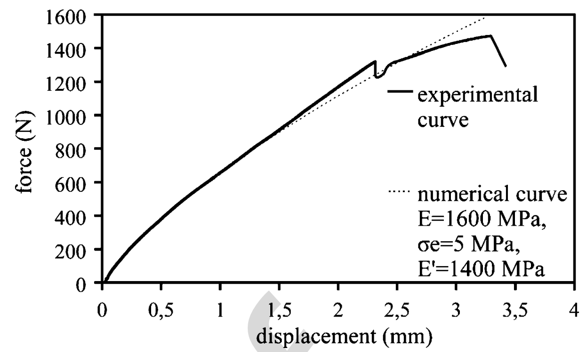

Fig. 6. Identification of bone material properties.

of the facial structure between the beginning of the test and the level load of 1005 N was an association of two structure displacements (Fig. 7).

- A translation in the vertical loading direction, which was maximal under the loading plate.
- A rotation, characterized by an horizontal displacement toward the vertex for the lower part of the face and toward the mandible for the upper part. A maximum value was observed for the thinner part of the zygomatic arch as well as for the sphenoid bone.

Two facial components acted as reinforcement pillars during the loading: the zygomatic arch which bent on its smaller section due to the loading orientation unaligned to the arch axis, and the orbital edge which was submitted to tensile loading. Then, limited forces were transmitted to the skull through the frontal and the sphenoid bones.

First, a qualitative comparison was made between experimental results and model's response. To obtain a clear representation of the experimental and numerical displacement distributions, scales were adjusted separately. The 2-D movements shown by the finite element model for this test simulation are similar to displacements of anatomical part described above: maximal values had the same location and displacement signs were equivalent [Fig. 7(c) and (d)]. However, for the horizontal direction, the maximal displacement located on zygomatic arch was larger in the numerical simulation.

Quantitatively, the experimentally measured horizontal displacements ranged from -0.06 to 0.06 mm. These values were too small to be analyzed accurately since they were approaching the measurement accuracy and then the relative error was not calculated for this measurement direction. The experimentally measured vertical displacements varied between 0.14 mm on skull to 0.47 mm on zygomatic bone. The minimal value was high considering its location which was far from the loading plate and near the fixed boundary conditions. The vertical displacements computed using the finite element model had a larger range from -0.1 mm on skull to 0.9 mm on zygomatic bone. The relative error of vertical displacements varied between 8% on the lower part of the zygomatic arch to 70% on the upper part of zygomatic arch (Fig. 8). The minimal error of 8% is obtained for measured and computed vertical displacements, respectively, equal to 0.25 mm and 0.229 mm. The relative

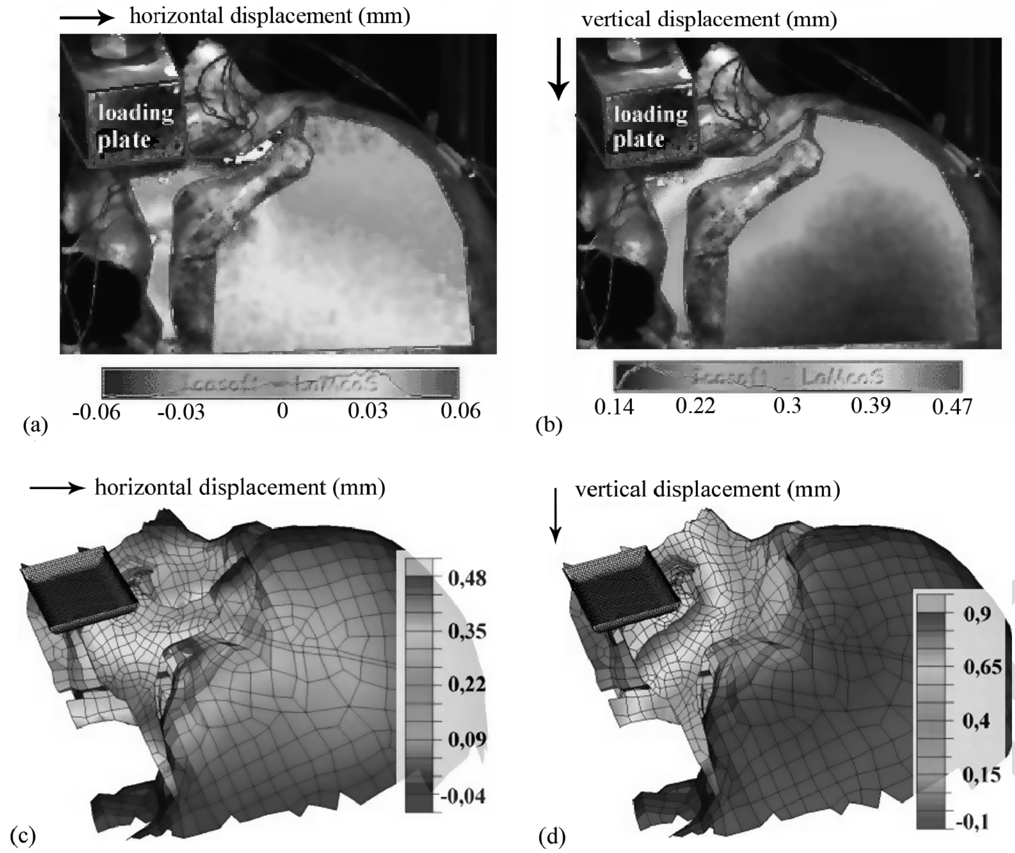

Fig. 7. Measured and computed 2-D displacements of the lateral part of the head skeleton. (a) Distribution of horizontal displacements on anatomical part. (b) Distribution of vertical displacements on anatomical part. (c) Distribution of horizontal displacements on model. (d) Distribution of vertical displacements on model. (Color version available online at http://ieeexplore.ieee.org.)

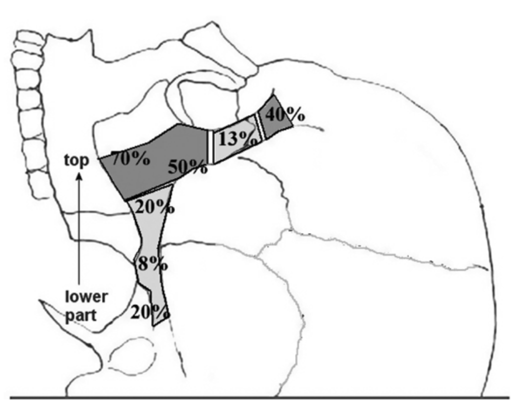

(a)

position	Usim (mm)	Uexp (mm)	er (%)
lower part	0.148427	0.231	35.74
	0.181027	0.239	24.25
	0.209653	0.2489	15.76
	0.229181	0.25	8.32
	0.277674	0.245	-13.33
	0.288677	0.26	-11.03
	0.417896	0.324	-28.98
	0.397703	0.279	-42.54
	0.397301	0.329	-20.76
	0.653078	0.39	-67.45
	0.611181	0.377	-62.11
	0.536483	0.359	-49.43
	0.778555	0.46	-69.25
	0.735418	0.431	-70.63
	0.68432	0.41	-66.9
top	0.639913	0.395	-62

(b)

Fig. 8. Distribution of the relative error for computed vertical displacement of the lateral part of the head skeleton. (a) Schema of the distribution. (b) Summary table.

error of 70% corresponds to measured and computed values of 0.43 mm and 0.73 mm, respectively.

IV. Discussion and Conclusion

The finite element model of the human head skeleton presented in this paper is based on an accurate geometric reconstruction performed using CT scan slices. The fine scan resolution and step slice, as well as the variable density of the mesh allowed a good accuracy of the bone structure representation. Moreover, since thickness is an important parameter in structure behavior under loading, the allocation of real thickness to elements ensures more accuracy in mechanical behavior simulation. In view of using the model for dynamical simulations as well as for static computation, a particular care was taken to avoid the use of three nodes elements and to limit the number of elements for a reasonable computational time.

The loading location and direction chosen for static compression tests is compatible with a realistic car crash situation.

The 30° oriented loading on zygomatic bone corresponds to the impact conditions of face on the steering wheel when the car does not have an air bag and the driver wears his seat belt. The first rupture of bone structure occurred for a force value equal to 1319 N which is close to those given by Allsop (1737.5 N) for impact tests with fixed boundary conditions [6]. The quite large range observed in rupture values is linked to the test conditions (boundaries, static or dynamic test, velocity) and to the anatomical part characteristics such as morphology, age and gender of the subject, absence of soft tissues. The values for the mechanical parameters obtained by identification from the experimental curve are the elasto-plastic properties of the whole bone structure ($\mathrm{E} = 1600$ MPa, $\sigma\mathrm{e} = 5$ MPa, and $\mathrm{E}' = 1400$ MPa).When comparing these values to literature on mechanical properties of cranial bone, they correspond to minimal values of interval given by Delille [24], who performed bending tests and identification of elasto-plastic properties on 67 samples coming from 12 subjects. The Young's modulus is also in the range of values obtained by McElhaney *et al.* [23].

The model's behavior was compared to the displacement field measurements obtained using a digital image correlation technique. Qualitatively, the displacement distribution simulated with the model is very similar to the real one, even if the maximum value of the zygomatic arch's horizontal displacement is more localized in the experiment than in the simulation. This is due to the difference in zygomatic arch morphology since the tested and modeled head do not watch exactly. In fact, the narrower part of the real zygomatic arch shows the maximum horizontal displacement value because of bending movement. On the model the shape of the arch does not include this narrow section. Quantitatively, the measured and computed vertical displacements were close on the zygomatic arch and on the orbit edge. A large error is found on the skull and the upper part of the zygomatic bone. Several phenomena explain these results for the quantitative comparison. First, the experimental displacements measured on this area are subjected to limitations. The displacement field obtained using the digital image correlation technique was measured in a plane which was chosen parallel to the zygomatic arch. The orbit edge is also parallel to this plane whereas the cranial part and the upper area of the zygomatic bone are out of plane. Thus, external plane displacements may disturb the experimental measurements and the local comparison in these two areas. Moreover, the displacements measured are small and sometimes they are close to the measurement accuracy, as those located on the skull, near the fixed boundary conditions. Second, as we saw for the qualitative comparison, the structure geometry is an important factor which introduces some bias in local comparison between anatomical part and model's behavior. In fact, the geometrical variability is high between one subject and another; this may disturb the mechanical response as well as the location of boundary and loading conditions.

This new measurement technique adapted to anatomical part of the body presents some limitations due to the specificity of the tested object. Nevertheless, on an appropriate measurement area, it brings important information that shows first a good qualitative correspondence, and second a small relative error equal to 8% between anatomical part and finite element model. Thus, this comparison allows the validation of our finite element model of the human head skeleton.

In the literature, the assessment of models of the head bone structure is usually based on the comparison of global curves (force/displacement or acceleration/time) since local data are not easy to acquire. Moreover, boundary and loading conditions of some experiments used for validation are not described accurately (padding, neck effect, etc.) and are difficult to simulate.

The new assessment method presented in this paper contributes to improve the validation of finite element model since it is divided into two steps: the adjustment of numerical to experimental data measured on the loading point which is commonly used, and then a local validation performed using a digital correlation method on a large area of the structure. Further investigations will be carried out to adapt the digital correlation technique to 3-D measurements and to dynamical loading. Our finite element model of human head skeleton was validated using this assessment method under static loading and is now available for a large field of applications.

ACKNOWLEDGMENT

The authors would like to thank P. Clerc (Mecanium SARL) for the realisation of digital correlation measurements, P. Lapellerie for his contribution to the PMHS experiments, and Dr. F. Cotton for the CT scan.

REFERENCES

[1] F. Roccia, F. Servadio, and G. Gerbino, "Maxillofacial fractures following air bag deployment," *J. Cranio-Maxillofacial Surg.*, vol. 27, pp. 335–338, 1999.
[2] K. Hussain, D. B. Wijetunge, S. Grubnic, and I. T. Jackson, "A comprehensive analysis of craniofacial trauma," *J. Trauma*, vol. 36, no. 1, pp. 34–46, 1994.
[3] Association for the Advancement of Automotive Medicine, Barrington, IL, The Abbreviate Injury Scale, Update 98 1998.
[4] B. Laumon, Recherches coordonnées sur les traumatismes consécutifs à un accident de la circulation routière, et sur leurs causes et conséquences 0206, 2002, p. 292, 129.
[5] A. M. Nahum, J. D. Gatts, C. W. Gadd, and J. Danforth, "Impact tolerance of the skull and face," in *Proc. 12th Stapp Car Crash Conf.*, Detroit, MI, 1968, pp. 302–316.
[6] D. L. Allsop, C. Y. Warner, M. G. Wille, D. C. Schneider, and A. M. Nahum, "Facial impact response- a comparison of the hybrid III dummy and human cadaver," in *Proc. 32nd Stapp Car Crash Conf.*, Atlanta, GA, 1988, pp. 139–155.
[7] N. Yoganandan, A. Sances, F. A. Pintar, D. J. Maiman, D. C. Hemmy, S. J. Larson, and V. M. Haughton, "Traumatic facial injuries with steering wheel loading," *J. Trauma*, vol. 31, no. 5, pp. 699–710, 1991.
[8] G. W. Nyquist, J. M. Cavanaugh, S. J. Goldberg, and A. I. King, "Facial impact tolerance and response," presented at the Stapp Car Crash Conf., 1988, Paper 861896.
[9] M. Claessens, *Finite Element Modeling of the Human Head Under Impact Conditions*. Eindhoven, The Netherlands: Technishe Universiteit Eindhoven, 1997, p. 137.
[10] H. Y. Choi, S. H. Lee, I. H. Lee, and E. Haug, "Finite element modeling of human head-neck complex for crashwortiness simulation," in *Proc. Conf. Computational Fluid and Solid Mechanics*, 2001, pp. 114–119.
[11] H. Iseri, A. E. Tekkaya, O. Ostan, and S. Bigic, "Biomechanical effects of rapid maxillary expansion on the craniofacial skeleton, studied by the finite element method," *Eur. J. Orthodont.*, vol. 20, pp. 347–356, 1998.
[12] U. Hartmann, F. Kruggel, T. Hierl, G. Lonsdale, and R. Klöppel, "Skull mechanic simulations with the prototype SimBio environment," in *Proc. Conf. Computational Fluid and Solid Mechanics*, 2001, pp. 243–246.
[13] T. J. Horgan and M. D. Gilchrist, "The creation of three-dimensional finite element models for simulating head impact biomechanics," *Int. J. Crashworthiness*, vol. 8, no. 4, pp. 353–366, 2003.
[14] L. Zhang, K. H. Yang, R. Dwarampudi, K. Omori, T. Li, K. Chang, W. N. Hardy, T. B. Khalil, and A. I. King, "Recent advances in brain injury research: a new human head model development and validation," *Stapp Car Crash J.*, vol. 45, pp. 369–393, 2001.

[15] Kang, R. Willinger, and B. M. Diaw, "Validation of a 3D anatomic human head model and replication of head impact in motorcycle accident by finite element modeling," presented at the 41st Stapp Car Crash Conf., 1997.
[16] R. Willinger, B. M. Diaw, and H. S. Kang, "Finite element modelling of skull fractures caused by direct impact," *Int. J. Crashworthiness*, vol. 5, no. 3, pp. 249–258, 2000.
[17] K. Tanne, S. Matsubara, and M. Sakuda, "Location of the centre of resistance for the nasomaxillary complex studied in a three-dimensional finite element model," *Br. J. Orthod.*, vol. 22, no. 3, pp. 227–232, 1995.
[18] H. Jinushi, T. Suzuki, T. Naruse, and Y. Isshiki, "A dynamic study of the effect on the maxillofacial complex of the face bow: analysis by a three-dimensional finite element method," *Bull. Tokyo Dent. Coll.*, vol. 38, no. 1, pp. 33–41, 1997.
[19] B. Autuori, K. Bruyère-Garnier, F. Morestin, M. Brunet, and J. P. Verriest, "Assessment of a finite element model of the human facial bone structure," in *27e Congrès de la Société de Biomécanique*, Valenciennes, France, Sep. 2002, vol. 110, Archives of physiology and biochemistry, p. 36.
[20] S. Mguil-Touchal, F. Morestin, and M. Brunet, "Various experimental applications of digital image correlation method," in *Proc. CMEM 97*, 1997, pp. 45–58.
[21] P. Clerc, F. Morestin, and M. Brunet, "Measurement of deformation fields using numerical images correlation," in *Proc. AMPT'99 IMC16*, 1999, vol. 3, pp. 1889–1897.
[22] K. Bruyere, F. Bermond, R. Bouquet, Y. Caire, M. Ramet, and E. Voiglio, "Human Maxilla bone response to 30 ° oriented impacts and comparison with frontal bone impacts," presented at the 44th Association for the Advancement of Automotive Medicine (AAAM) Conf., , Chicago, IL, Oct. 2–4, 2000.
[23] J. H. McElhaney, J. L. Fogle, J. W. Melvin, R. R. Haynes, V. L. Roberts, and N. M. Alem, "Mechanical properties of cranial bone," *J. Biomech.*, vol. 3, pp. 495–511, 1970.
[24] C. Dellile, "Contribution à l'identification de lois matérielles de l'os du crâne humain en quasi-statique à partir d'expérimentations et de simulations numériques," in *Génie Mécanique*. Valenciennes, France: Université de Valenciennes et du Haut Cambrésis, 2002, p. 190.

Barbara Autuori received the Ph.D. degree for the development of a finite element model on the human facial skeleton, from INSA, Lyon, France, in April 2004.

She was involved in the Science and Technology in the Transport Safety (ST2) project as a Postdoctoral Researcher at the Laboratory of Industrial and Human Automation, Mechanics and Computer Science, Valenciennes, France. Her job was to evaluate the injury risk of car drivers in precrash situation.

Karine Bruyère-Garnier Please provide biographical information (and photo if available).

Fabrice Morestin Please provide biographical information (and photo if available).

Michel Brunet Please provide biographical information (and photo if available).

Jean-Pierre Verriest Please provide biographical information (and photo if available).